Competing Structural Instabilities in Cubic Perovskites

W. Zhong and David Vanderbilt
Department of Physics and Astronomy, Rutgers University, Piscataway, New Jersey 08855-0849
(Received 17 November 1994)

We study the antiferrodistortive instability and its interaction with ferroelectricity in cubic perovskite compounds. Our first-principles calculations show that coexistence of both instabilities is very common. We develop a first-principles scheme to study the thermodynamics of these compounds when both instabilities are present, and apply it to $SrTiO_3$. We find that increased pressure enhances the antiferrodistortive instability while suppressing the ferroelectric one. Moreover, the presence of one instability tends to suppress the other. A very rich P-T phase diagram results.

PACS numbers: 77.80.Bh, 61.50.Lt, 64.60.Cn, 64.70.–p

The great fascination of the cubic perovskite structure is that it can readily display a variety of structural phase transitions, ranging from nonpolar antiferrodistortive (AFD) to ferroelectric (FE) and antiferroelectric in nature [1]. The competition between these different instabilities evidently plays itself out in a variety of ways, depending on the chemical species involved, leading to the unusual variety and richness of the observed structural phase diagrams. Moreover, all the phase transitions involve only small distortions from the ideal cubic structure, and are therefore appealing objects for experimental and theoretical study. However, our microscopic understanding of the chemical origins of these instabilities and of their interactions is still very limited.

Thus, there is a pressing need for accurate, chemically specific investigations of the structural energetics of these compounds, leading to a detailed understanding of the phase transition behavior. Previous phenomenological model Hamiltonian approaches [2–5] have been limited by oversimplification and ambiguities in interpretation of experiment, while empirical [6] and nonempirical pair-potential methods [7] have not offered high enough accuracy. First-principles density-functional calculations have been shown to provide accurate total-energy surfaces for perovskites as regards FE distortions [8–10]. However, to our knowledge, there have been no previous first-principles studies of AFD distortions, and therefore no detailed microscopic theories of the phase transformation behavior.

Here, we build upon previous work in which a fully first-principles scheme was used to study the FE transitions in $BaTiO_3$, leading to an accurate microscopic understanding of the phase transition sequence [11]. In the present work, we develop a similar approach which is capable of treating simultaneously the FE and AFD degrees of freedom, allowing for the first time a detailed *ab initio* study of the phase behavior for perovskites in which both instabilities are present. We present systematic calculations of the susceptibility against R-point zone-boundary AFD modes for a set of eight compounds, demonstrating that the AFD instability is very common. Then, we briefly describe our first-principles scheme for studying finite-temperature properties, and apply it to $SrTiO_3$. We study the evolution of the phonon instabilities with temperature, and calculate the P-T phase diagram. In so doing, we compute the interactions between the AFD and FE instabilities, and expose their implications for the thermodynamic properties.

The high-symmetry ABO_3 perovskite structure is simple cubic with O atoms at the face centers and metal atoms A and B at the cube corner and body center, respectively. The two most common instabilities result from a softening of either a zone-center polar phonon mode (FE) or a nonpolar zone-boundary mode (AFD) involving rigid rotations of oxygen octahedra. These modes are illustrated in the left and right insets, respectively, in Fig. 1. $BaTiO_3$ is a classical example of the first type, while the best-known example of the second kind is the $T = 105$ K transition in $SrTiO_3$ [5], which results from a softening of a Γ_{25} phonon at R $[(111)\pi/a]$.

The stability of perovskite compounds against R-point phonon distortions can be expressed in terms of a stiffness $\kappa^R = \frac{1}{2}\partial^2 E/\partial\phi^2$, where ϕ is the rotation angle of the oxygen octahedra. To obtain κ^R, we perform frozen

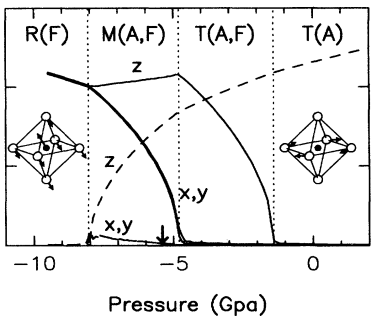

FIG. 1. $T = 0$ order parameters vs pressure for $SrTiO_3$. Solid and dashed lines denote Cartesian components of $\mathbf{f}(\Gamma)$ and $\mathbf{a}(R)$, respectively. Phases are labeled by lattice symmetry (R = rhombohedral, M = monoclinic, T = tetragonal, O = orthorhombic) and by instabilities present (A =antiferrodistortive, F = ferroelectric). Dotted lines denote phase boundaries. Vertical arrow indicates theoretical pressure P_0 at which the lattice constant matches the experimental $P = 0$ one. Left inset: sketch of displacements leading to $R(F)$ phase (Sr is omitted for clarity). Right inset: same for $T(A)$ phase.

0031-9007/95/74(13)/2587(4)$06.00

TABLE I. Calculated stiffness κ^R of R-point AFD phonon mode (in Hartree), and tolerance factor t, for several perovskite compounds.

	κ^R	t		κ^R	t
$BaTiO_3$	0.295	1.07	$SrTiO_3$	−0.042	1.01
$KNbO_3$	0.242	1.06	$NaNbO_3$	−0.133	0.97
$BaZrO_3$	−0.021	1.01	$PbZrO_3$	−0.324	0.97
$PbTiO_3$	−0.037	1.03	$CaTiO_3$	−0.375	0.97

phonon calculations using density-functional theory within the local-density approximation (LDA) and Vanderbilt ultrasoft pseudopotentials [12]. In Table I, we list values of κ^R for a set of eight compounds, calculated at the experimental lattice constants [13] as listed in Ref. [10]. Negative values indicate instability to R-point phonon distortions.

Table I shows that the tendency towards AFD instability is strongly correlated with trends in ionic radii. Such trends in an ABO_3 compound are conventionally described by a tolerance factor $t = (r_A + r_O)/\sqrt{2}(r_B + r_O)$. Values for t are given in Table I, using the ionic radii of Ref. [14]. We find that κ_R is almost monotonic with t; i.e., a larger A or a smaller B atom tends to stabilize the cubic structure. This simple behavior contrasts with the case of the ferroelectric instability, where covalent interactions play an important role [15].

Inspecting Table I, we see that the two compounds $BaTiO_3$ and $KNbO_3$ are clearly stable with respect to AFD distortions, consistent with experimental observations. (Both materials undergo a similar series of FE transitions.) On the other extreme, we find that $CaTiO_3$, $PbZrO_3$, and $NaNbO_3$ have a strong AFD instability. All three compounds are also predicted to have FE instabilities [10], consistent with the observation of complex phase diagrams and high transition temperatures in all three cases. Finally, our calculations for $SrTiO_3$, $PbTiO_3$, and $BaZrO_3$ show a weak AFD instability. $PbTiO_3$ is observed to go through a weak unidentified transition at $T = 180$ K [16] which could be AFD related. $BaZrO_3$ is observed to remain cubic down to $T = 0$; the weak instability predicted by our calculation could be suppressed by quantum zero-point fluctuations. For $SrTiO_3$, we predict a weak AFD instability consistent with a low T_c of 105 K observed for its cubic-to-AFD transition.

The above calculations indicate that coexistence of FE and AFD instabilities is very common in perovskites. To study the consequence of such a situation, we have chosen to study the case of $SrTiO_3$ in depth. Our first-principles scheme can be explained briefly as follows. The energy is Taylor expanded in low-energy distortions, with expansion parameters determined from LDA calculations. The resulting Hamiltonian is studied using Monte Carlo (MC) simulations. The low-energy distortions we included are those connected with zone-center FE-like modes, zone-boundary AFD-like modes, and strain. To do this we construct a FE "local mode" such that a uniform arrangement of local mode amplitudes $\mathbf{f}_l$ reproduces the softest zone-center Γ_{15} (FE) modes (l is a cell index). Similarly, we construct an AFD local mode (a local rotation of an oxygen octahedron) so that a staggered arrangement of amplitudes $\mathbf{a}_l$ reproduces the $\Gamma_{25}(R)$ mode. Finally, the local strains are represented in terms of a displacement vector $\mathbf{u}_l$.

Thus, we have three vector degrees of freedom $\mathbf{f}_l$, $\mathbf{a}_l$, and $\mathbf{u}_l$ per cell. The energy terms retained in our Taylor expansion of the potential energy are as follows: (i) on-site self-energy, up to quartic anharmonic order for $\mathbf{f}_l$ and $\mathbf{a}_l$, and up to harmonic order for $\mathbf{u}_l$ (elastic energy); (ii) harmonic intersite interactions between $\mathbf{f}_l$ (including long-range dipole-dipole interactions) and $\mathbf{a}_l$ (short-range only); and (iii) on-site coupling energy to the lowest order between $\mathbf{a}_l$ and $\mathbf{u}_l$, between $\mathbf{f}_l$ and $\mathbf{u}_l$, and between $\mathbf{f}_l$ and $\mathbf{a}_l$. The determination of the expansion parameters involves LDA calculations for supercells containing up to 20 atoms with low symmetry, using ultrasoft pseudopotentials [12]. The details of the Hamiltonian, the first-principles calculations, and the values of the expansion parameters will be presented elsewhere [17].

To obtain the structural and thermodynamic properties, we perform MC simulations on an $L \times L \times L$ cubic lattice with periodic boundary conditions [18]. The identification of different phases can be made by monitoring the FE order parameter $\mathbf{f}(\Gamma)$ (the Fourier transform of $\mathbf{f}_l$ at $\mathbf{k} = \Gamma$), and similarly the AFD order parameters $\mathbf{a}(R)$ and $\mathbf{a}(M)$ [$M = (110)\pi/a$]. $\mathbf{a}(M)$ is found to remain small for $SrTiO_3$, and will not be discussed further.

We first investigate the ground-state structure for $SrTiO_3$ as a function of hydrostatic pressure. We find it convenient to run the MC calculations at $L = 4$ at $T = 0.1$ K (finite-size and hysteresis effects are not important at low T). The calculated order parameters $\mathbf{a}(R)$ and $\mathbf{f}(\Gamma)$ are shown in Fig. 1. Zero pressure in the figure corresponds to the LDA-calculated equilibrium lattice constant, which is about 1% too small. Since both the FE and AFD instabilities are sensitive to lattice constant, comparison with the experimental phase diagram is best made with the zero of the pressure axis shifted by $P_0 = -5.4$ GPa (see arrow in Fig. 1), the value which restores the experimental lattice constant. From Fig. 1, we see that pressure has opposite effects on $\mathbf{a}(R)$ and $\mathbf{f}(\Gamma)$, and that as a function of pressure the ground state of $SrTiO_3$ can have four phases. The cubic phase, which is stable at high temperature, is not present. At high pressure, only one component of $\mathbf{a}(R)$ is nonzero, indicating an AFD tetragonal structure ($I4/mcm$). As P is lowered, the corresponding (z) component of $\mathbf{f}(\Gamma)$ becomes nonzero, and the structure transforms to tetragonal with FE and AFD ($I4cm$). A further decrease of pressure creates a low-symmetry monoclinic structure (Pb), in which all components of $\mathbf{f}(\Gamma)$ and $\mathbf{a}(R)$ are nonzero. Finally, below −8 GPa the structure becomes FE rhombohedral ($R3m$). We see that the coexistence of zone-center and zone-boundary instabilities creates many different phases and complicated structures, even at $T = 0$.

At finite temperature, the behavior becomes even more interesting. We first show our MC simulation for $P = P_0$ (-5.4 GPa) and $L = 12$. We start at high temperature and decrease T in small steps, allowing the system to reach equilibrium at each step. The hysteresis and finite-size effects on the transition temperatures are found to be negligible. In Fig. 2, we show the order parameters $\mathbf{f}(\Gamma)$ and $\mathbf{a}(R)$ as a function of T. (Since the order parameter vectors may rotate, what we actually show are the averaged maximum, intermediate, and minimum components of each vector.) Naturally, the system is found to adopt the cubic structure at high temperature. As T is reduced, a transition to an AFD tetragonal structure occurs at 130 K, as indicated by a strong increase of $a_z(R)$. A second transition occurs at $T = 70$ K to a FE tetragonal structure, below which $f_z(\Gamma) > 0$. At very low temperature (10 K), the system transforms to the low-symmetry monoclinic structure.

Comparing with experiment, we see that our cubic-to-AFD(T) transition at 130 K corresponds very well to the observed one at 105 K [19]. Our observations of additional transitions to AFD + FE phases at 70 and 10 K are not, however, in direct accord with experiment. Instead, they agree with the observed softening of the FE polar phonons, which would extrapolate to a FE transition close to 40 K [20] or 20 K [21]. It has been speculated that the absence of a true FE phase at $T = 0$ is a result of quantum fluctuations of atomic positions, leading to crossover into a "quantum paraelectric phase" at very low temperature [20–22]. Our inability to obtain agreement between the classical MC theory and experiment at $T = 0$ lends additional support to this conclusion.

To construct a P-T phase diagram, we have carried out a series of similar cooling-down simulations at different pressures. As shown in Fig. 3, there are at least seven different phases present. At strong negative pressure, $SrTiO_3$ behaves rather like $BaTiO_3$, with a cubic → tetragonal → orthorhombic → rhombohedral sequence of transitions on cooling. Increasing the hydrostatic pressure tends to stabilize the AFD state and destabilize the FE one. The pressure coefficient $dT_c/dP = 28$ K/GPa at P_0 agrees well with the experimental value of 25 K/GPa [23]. At very high pressure, the system undergoes a single transition to a tetragonal AFD structure. In the intermediate regime, the presence of both kinds of instabilities creates a variety of phases, including the complicated monoclinic structure. The ordering of the FE and AFD transition temperatures reverses ~1.5 GPa below P_0 (hatched area in Fig. 3). In this critical region the AFD and FE transition temperature change dramatically, and the system may possess some interesting characteristics (e.g., extreme dielectric properties).

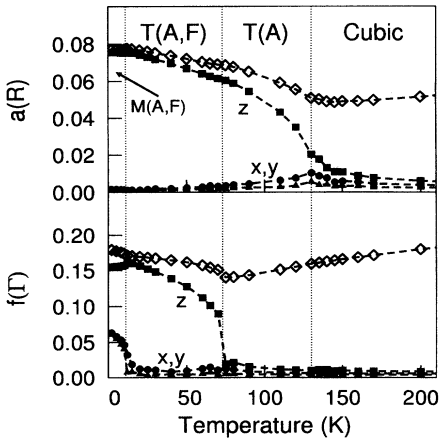

FIG. 2. Order parameters of $SrTiO_3$ vs T at $P_0 = -5.4$ GPa. Upper panel: averaged largest, middle, and smallest Cartesian components of $\mathbf{a}(R)$. Lower panel: corresponding quantities for $\mathbf{f}(\Gamma)$. Phase labels are the same as in Fig. 1.

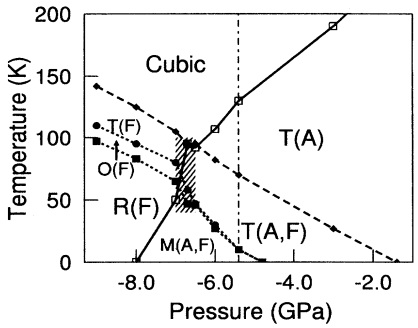

FIG. 3. P-T phase diagram of $SrTiO_3$. Hatching indicates the critical region where dramatic changes occur. Vertical dash-dotted line indicates the pressure P_0 corresponding to experimental $P = 0$. Phase labels are the same as in Fig. 1.

The dramatic reversal of the AFD and FE transition temperatures in the hashed region of the P-T phase diagram suggests the presence of a competition between the two instabilities. Our first-principles theory confirms this and provides microscopic insight into the competition. The FE and AFD instabilities affect each other mainly through the on-site anharmonic coupling, and through their mutual coupling to the elasticity. In $SrTiO_3$, the on-site coupling is found to lead the FE and AFD modes to suppress one another, while the coupling through strain tends to stabilize tetragonal phases relative to other phases. Our calculations show that the former effect dominates.

One way of quantifying the importance of this competition is to compare with what would happen if the FE or AFD degrees of freedom were artificially frozen out. We find that at P_0, the AFD transition temperature would be 25% higher if all $\mathbf{f}_l$ were frozen to zero; conversely, the FE C-T transition would be 20% higher if all $\mathbf{a}_l = 0$. At $T = 0$, freezing $\mathbf{f}_l = 0$ reduces the cubic-to-AFD transition pressure from -8 to -11.8 GPa, while freezing $\mathbf{a}_l = 0$ increases the cubic-to-FE transition from -1.5 to 0.8 GPa. Thus, we see clearly that the FE and AFD instabilities compete with and tend to suppress one another. Because of this competition, the $T(A,F)$ phase at P_0 is only slightly more stable than the $T(A)$ phase,

even at $T = 0$; the energy surface relative to the FE distortion takes the form of a very long and shallow double well. This may help explain the observed suppression of the ferroelectric phase by quantum fluctuations [20–22].

Much of the interesting portion of our phase diagram appears to the left of P_0, i.e., at negative (inaccessible) physical pressures. It would be interesting, therefore, to consider compounds such as $CaTiO_3$ or $NaNbO_3$ which are FE at P_0, and study AFD instabilities at elevated P. While the exact details of our phase diagram for $SrTiO_3$ should not be expected to carry over to other perovskites, we expect the general features to persist, especially the tendency of the FE and AFD instabilities to suppress each other and the presence of complicated phase diagrams with numerous phases.

In conclusion, we have performed a fully first-principles study of the finite-temperature properties of perovskite compounds with both FE- and AFD-type instabilities. We find that AFD instabilities are almost as common as FE ones in cubic perovskite compounds. For $SrTiO_3$, our calculated P-T phase diagram shows that the FE and AFD instabilities have opposite trends with pressure. The anharmonic on-site coupling between order parameters causes the AFD and FE instabilities to tend to suppress one another.

We thank R. D. King-Smith and K. M. Rabe for discussions. This work was supported by ONR Grant N00014-91-J-1184. Partial supercomputing support was provided by NCSA Grant DMR920003N.

[1] M. E. Lines and A. M. Glass, *Principles and Applications of Ferroelectrics and Related Materials* (Clarendon Press, Oxford, 1977).
[2] M. T. Dove, A. P. Giddy, and V. Heine, Ferroelectrics **136**, 33 (1992).
[3] E. Pytte, Phys. Rev. B **5**, 3758 (1972).
[4] A. D. Bruce and R. A. Cowley, *Structural Phase Transitions* (Taylor & Francis, London, 1981).
[5] E. Pytte and J. Feder, Phys. Rev. **187**, 1077 (1969); J. Feder and E. Pytte, Phys. Rev. B **1**, 4803 (1970).
[6] H. Bilz, G. Benedek, and A. Bussmann-Holder, Phys. Rev. B **37**, 4840 (1987), and references therein.
[7] G. Gordon and Y. S. Kim, J. Chem. Phys. **56**, 3122 (1972); L. L. Boyer *et al.*, Phys. Rev. Lett. **54**, 1940 (1985); P. J. Edwardson *et al.*, Phys. Rev. B **39**, 9738 (1989).
[8] R. E. Cohen and H. Krakauer, Phys. Rev. B **42**, 6416 (1990); R. E. Cohen and H. Krakauer, Ferroelectrics **136**, 65 (1992); R. E. Cohen, Nature (London) **358**, 136 (1992).
[9] D. J. Singh and L. L. Boyer, Ferroelectrics **136**, 95 (1992).
[10] R. D. King-Smith and D. Vanderbilt, Phys. Rev. B **49**, 5828 (1994); Ferroelectrics **136**, 85 (1992).
[11] W. Zhong, D. Vanderbilt, and K. M. Rabe, Phys. Rev. Lett. **73**, 1861 (1994); (unpublished).
[12] D. Vanderbilt, Phys. Rev. B **41**, 7892 (1990).
[13] Since κ^R is pressure sensitive, using experimental lattice constants avoids the error due to $\sim 1\%$ underestimate of the LDA lattice constants.
[14] R. Shannon, Acta Crystallogr. Sect. A **32**, 751 (1976).
[15] W. Zhong, R. D. King-Smith, and D. Vanderbilt, Phys. Rev. Lett. **72**, 3618 (1994).
[16] J. Kobayashi, Y. Uesu, and Y. Sakemi, Phys. Rev. B **28**, 3866 (1983).
[17] W. Zhong and D. Vanderbilt (unpublished).
[18] M. P. Allen and D. J. Tildesley, *Computer Simulation of Liquids* (Oxford, New York, 1990); *The Monte Carlo Method in Condensed Matter Physics,* edited by K. Binder (Springer-Verlag, Berlin, 1992).
[19] G. Shirane and Y. Yamada, Phys. Rev. **177**, 858 (1969); W. Buyers and R. Cowley, Solid State Commun. **7**, 181 (1969).
[20] K. A. Müller and H. Burkard, Phys. Rev. B **19**, 3593 (1979); K. A. Müller, W. Berlinger, and E. Tosatti, Z. Phys. B **84**, 277 (1991).
[21] R. Viana *et al.*, Phys. Rev. B **50**, 601 (1994).
[22] R. Martonak and E. Tosatti, Phys. Rev. B **49**, 12 596 (1994).
[23] B. Okai and J. Yoshimoto, J. Phys. Soc. Jpn. **39**, 162 (1975).